Materials Transactions, Vol. 61, No. 10 (2020) pp. 1940 to 1948

Kinetic Analysis for Agglomeration-Flotation of Finely Ground Chalcopyrite: Comparison of First Order Kinetic Model and Experimental Results

Vothy Hornn[1,*1,*2], Mayumi Ito[2], Ryosuke Yamazawa[1,*2], Hiromasa Shimada[1,*2], Carlito Baltazar Tabelin[2,*3], Sanghee Jeon[2], Ilhwan Park[2] and Naoki Hiroyoshi[2]

[1]*Division of Sustainable Resources Engineering, Graduate School of Engineering, Hokkaido University, Sapporo 060-8628, Japan*
[2]*Division of Sustainable Resources Engineering, Faculty of Engineering, Hokkaido University, Sapporo 060-8628, Japan*

Particle size-flotation rate relationships can be discussed by a first-order kinetic model for flotation, which considers the probability of particle-bubble collision, attachment and detachment; and it was confirmed that recovery rate of finely ground hydrophobic particles in the froths are very low because of the limited particle-bubble collision probabilities. One method to improve the flotation of fine minerals is to agglomerate them before flotation using oil as a bridging liquid, an approached that has been shown to improve the flotation rates dramatically. A mathematical kinetic model for the flotation of agglomerated particles would be useful to design and optimize the agglomeration-flotation process, but no generally applicable model has been established yet. In this paper, flotation experiments of finely ground chalcopyrite were carried out with and without oil-agglomeration as pretreatment and the kinetic data (time-recovery curves) were compared with the conventional first-order kinetic model for flotation. Without agglomeration, time-recovery curves determined by the experiments fitted well with the model calculations, but there were significant deviations between experimental results and model calculations for the agglomerated particles; that is, experimental flotation recoveries were much higher than those calculated by the model. The conventional first-order kinetic model does not consider particle size changes during flotation while the experimental results suggested that the size of agglomerates increased in the flotation cell. This may be one of the reasons why significant deviations between the experimental and modelling results were observed, suggesting that the kinetic model for agglomeration-flotation need to consider the growth of agglomerates during flotation.
[doi:10.2320/matertrans.M-M2020843]

(Received March 19, 2020; Accepted July 20, 2020; Published September 25, 2020)

Keywords: *flotation, agglomeration, chalcopyrite, first-order kinetic model*

1. Introduction

Flotation is the most commonly used mineral processing technique to recover and concentrate metal-sulfide minerals (e.g., chalcopyrite, molybdenite, galena and sphalerite) from their ores. Despite its widespread application, the efficiency of flotation dramatically decreases when particle sizes drop below the sub-sieve levels (<38 μm).[1)] For example, Trahar (1981) studied chalcopyrite–quartz flotation and reported that recovery of chalcopyrite decreased when the median particle size decreased from 20 to 3 μm.[2)] This low recovery of fine particles during flotation has been attributed by many authors to the low collision probability between fine mineral particles and air bubbles.[3–5)] Fine particles have small mass and momentum, so their motion simply follows the flow of water around rising air bubbles. This phenomenon severely limits fine particle collision with the bubble's surface, leading to substantial losses of recoverable minerals. Mathematically, particle-bubble collision probability, P_c, is expressed by

$$P_c = A\left(\frac{D_p}{D_b}\right)^n \quad (1)$$

where D_p and D_b are the particle and bubble diameters, respectively, and A and n are empirical constants that depend on the flow regime.[6)] As explained earlier, the probability of collision dramatically decreases as the size of a particle becomes very small ($D_p \ll D_b$).

*[1]Corresponding author, E-mail: vothytalis1102@yahoo.com
*[2]Graduate Student, Hokkaido University
*[3]Present address: School of Minerals and Energy Resources Engineering, The University of New South Wales, Sydney, NSW 2052, Australia

Many studies have suggested ways to get around this problem of poor fine particle recovery in flotation using two approaches: (1) bubble size reduction, and (2) particle aggregation. Column flotation,[7)] microbubble flotation,[8)] electro-flotation[9)] and dissolved-air flotation[10)] are some examples of bubble size reduction approaches. Meanwhile, particle aggregation strategies include shear flocculation,[11)] carrier flotation,[12)] polymer flocculation[13)] and oil-agglomeration.[1)] All of these techniques have their own benefits and drawbacks, but from the perspective of economics, oil-agglomeration is the most promising because oil is relatively inexpensive, the process could be easily integrated into existing flotation circuits, and the technique could effectively improve the recovery of fines. Generally, oil-agglomeration refers to a technique or a process to increase the apparent particle size by agglomerating fine hydrophobic particles suspended in water using oil as a bridging liquid. The pretreatment of very fine minerals with agglomeration is usually followed by conventional flotation and this series of processes is loosely termed "agglomeration-flotation". This method has been extensively studied for coal[14,15)] and some sulfides mineral such as molybdenite,[1)] sphalerite and galena.[16)] In oil-agglomeration of sulfide minerals, a surface modifier, such as xanthate, is added to enhance the mineral's hydrophobicity, which improves agglomeration. House and Veal (1989), for example, carried out the agglomeration of fine chalcopyrite with a large amount of oil to improve flotation recovery.[18)] Other studies improved this technique by utilizing emulsified oil, an approach that reduced the amount of oil used for agglomeration-flotation dramatically.[18–20)]

Although previous studies have reported agglomeration-flotation as a promising technique to improve the floatability

of finely ground mineral particles by increasing its apparent size, flotation model for agglomerated particles has not been established yet. A mathematical model for the flotation kinetics of agglomerated particles would be useful to design and optimize the agglomeration-flotation process. In this paper, flotation experiments were carried out with and without oil-agglomeration, and the kinetic data obtained were analyzed using the conventional first-order kinetic model for flotation. Kinetic analysis of finely ground chalcopyrite during agglomeration-flotation was carried out to identify the factors and important parameters affecting the process for future establishment of a flotation model for agglomerated mineral particles.

2. Materials and Methods

2.1 Minerals and reagents

The chalcopyrite sample used in this study was obtained from Copper Queen Mine, Arizona, USA. The sample was crushed by a jaw crusher, ground in a ball mill, and sieved to less than 75 μm. The ground sample was then further purified by heavy liquid separation using sodium polytungstate ($Na_6(H_2W_{12}O_{40})$) solution (specific gravity of 3) to remove light gangue minerals like quartz. After heavy liquid separation, the sample was washed with 1 M HNO_3, rinsed thoroughly with deionized water, and dewatered with acetone under vacuum following the procedure employed by several authors to remove oxidation products on pyrite.[21–23] The sample was analyzed by X-ray powder diffraction (XRD) (Multiplex, Rigaku Corporation, Japan) and X-ray fluorescence spectroscopy (XRF) (EDXL300, Rigaku Corporation, Japan), and the results showed that the sample is composed of 85% chalcopyrite with moderate to trace amounts of sphalerite, quartz and actinolite as gangue minerals (the XRF and XRD data were shown in supplementary data Table S1 and Fig. S1). Before flotation or agglomeration-flotation, the washed sample was finely ground in a vibratory disc mill (RS100, Retsch Inc., Germany) to obtain samples having three different D_{50} (3, 10 and 22 μm measured in ethanol).

Potassium amyl xanthate (KAX) (Tokyo Chemical Industry Co., Ltd., Japan) was used as the surface modifier to improve the hydrophobicity of chalcopyrite before flotation and agglomeration. Kerosene (Wako Pure Chemical Industries, Ltd., Japan) was used as the "bridging" liquid of chalcopyrite particles, and methyl isobutyl carbinol (MIBC) (Tokyo Chemical Industry Co., Ltd., Japan) was used as the frother in flotation.

2.2 Flotation tests

Flotation tests of chalcopyrite samples were carried out using an agitator-type flotation machine (FT-1000, Heiko, Japan). A 20 g sample was suspended in 400 mL of distilled water (5% pulp density). A 200 g/t of KAX was added and stirred for 5 min in a flotation cell to improve the hydrophobicity of chalcopyrite. After conditioning with KAX, the frother (25 μL/L of MIBC) was added and the pulp was stirred for another 3 min and then flotation was carried out at a flow rate of 1 L/min followed by separate collection of froth products within the following time intervals: 0–0.5, 0.5–1, 1–2, 2–4, 4–7, and 7–10 min. All of the froth products and the final tailing were oven dried (105°C) for 24 hours, weighed and analyzed by XRF for the copper (Cu) recovery calculation.

2.3 Agglomeration-flotation tests

A 20 g sample was suspended in 400 mL of distilled water (5% pulp density) and stirred for 5 min in a flotation cell after adding 200 g/t of KAX to improve the hydrophobicity of chalcopyrite. After conditioning with KAX, the suspension was transferred to a high-speed mixer (SPB-600J, Cuisinart, USA) and 1.5 mL of kerosene-water emulsion (0.3 mL kerosene in 1.2 mL distilled water) was added, and then mixed for 30 min at a mixing speed of 15,000 rpm to promote agglomeration. The agglomeration products were transferred to the flotation cell, and then flotation was carried out following the method outlined in the previous subsection.

2.4 Particle size distribution measurements

The particle size distributions of samples suspended in water were analyzed using laser diffraction sizer (Microtrac® MT3300SX, Nikkiso Co., Ltd., Japan). Accuracy of size measurement was confirmed by a preliminary experiment using different size fraction of ground chalcopyrite sample prepared by sieving. To determine the particle size of primary particles (i.e., un-agglomerated particles), the sample was suspended in ethanol and sonicated to disperse the particles prior to measurements by laser diffraction.

2.5 Bubble size distribution and bubble rising velocity measurements

Bubble size distribution measurements in a flotation cell were carried out based on the visual technique developed by Grau and Heiskanen.[25] The bubbles were drawn from the flotation cell into viewing chamber made of a single-crystal quartz "window" where undistorted pictures of bubbles could be captured using a high-speed (2000 frame per seconds) digital camera (HAS-L1, DITECT, Japan). The captured images were analyzed using an image analysis software (WinRoof v.5, MITANI Corporation, Japan). Before the measurement, the pulp for flotation of chalcopyrite (5% pulp density) was filtered to removed solid residues and the filtered solution was mixed with kerosene (0.75 mL/L). This solution was transferred to the flotation cell and after conditioning with 25 μL/L MIBC, air was injected to create bubbles for the measurements. The bubble rising velocities were also calculated from the change in position of the same bubble between 2 captured images from different frames.

2.6 Particle settling velocity measurements

For the measurement of particle settling velocity, agglomerated or un-agglomerated particle was suspended (0.1% pulp density) in a glass tube with a back-light source. Videos of settling particles were taken by a digital microscope (VHX-1000, Keyence Corporation, Japan) at 15 frames per second. The videos were then converted to images and the particle settling velocities were calculated based on settling distances of particles after 5 seconds.

3. The Kinetic Model for Flotation

3.1 Probability of particle collection by an air bubble

During flotation, suspended particles will collide with a rising bubbles and some of these particles will attach to the bubble surface and will travel upwards with the bubble.[27] The rate of collision of bubble-particles depends on many parameters such as the size of the bubble and the size of the particles, their relative velocities, and pulp density. The process of bubble–particle interaction during flotation is divided into three subprocesses, including collision, attachment, and detachment. The probability (P) of a particle being collected by an air bubble in the pulp phase of a flotation cell can be given by

$$P = P_c P_a (1 - P_d) \tag{2}$$

where P_c is the probability of bubble-particle collision, P_a is the probability of attachment and P_d is the probability of detachment.

For fine particles, P_d can be negligibly small because of the low inertia, so eq. (2) can be expressed as follows:

$$P = P_c P_a \tag{3}$$

P_c is determined by the hydrodynamics of the system, which is strongly affected by the particle size, bubble size and the turbulence of the system. P_a is also affected by the hydrodynamics but is largely a function of the surface chemistry involved. In this paper, $P_a = 1$ was used since chalcopyrite with KAX shows strong hydrophobic properties, in which case eq. (3) becomes:

$$P = P_c \tag{4}$$

In this paper, the model by Yoon and Luttrel[26] was used (eq. (5)).

$$P_c = \left[\frac{3}{2} + \frac{4{Re_b}^{0.72}}{15}\right]\left(\frac{D_p}{D_b}\right)^2 \tag{5}$$

where, Re_b is Reynold number of bubbles, D_b and D_p are bubble and particle diameters, respectively.

3.2 First-order kinetic model for flotation

Crushed samples have particle size distribution and these samples are treated by flotation. Recovery rate of targeted mineral as froth, R, can be calculated by using a conventional first-order kinetic model. The recovery of particle having dimeter D_{pi}, R_i as a function of time, t can be written as

$$\frac{dR_i}{dt} = k_i(1 - R_i) \tag{6}$$

$$R_i = 1 - e^{-k_i t} \tag{7}$$

where k_i is the kinetic constant. Recovery of target minerals having a particle size distribution η_i, R, can be written as

$$R = \sum \eta_i R_i = \sum \eta_i (1 - e^{-k_i t}) \tag{8}$$

In this study, measured size distributions of feed sample of flotation determined by laser diffraction were used for η_i, and the kinetic constant, k_i, was calculated as

$$k_i = n_b \times \frac{\pi}{4}(D_b + D_{pi})^2 (v_b + v_i) \times P_{ci} P_{ai} (1 - P_{di}) \tag{9}$$

Number of bubbles per unit volume, n_b was calculated as

$$n_b = \frac{G_v \tau_b}{(\pi/6){D_b}^3} \tag{10}$$

where, the specific aeration rate, G_v (m^3/s of air per m^3 cell volume) and average residence time of air bubble in the cell, τ_b [s] was calculated from v_b [m/s], $\tau_b = v_b/L$. Rising velocity of bubble (v_b) was calculated based on the equation proposed by King[27] and L [m] is the water height in flotation cell. P_{ci}, P_{ai}, P_{di} are the probability of collision, attachment and detachment of a particle having diameter, D_{pi}, respectively.

As described above, P_{di} is negligible and P_{ai} is almost one and this eq. (9) can be written as;

$$k_i = n_b \times \frac{\pi}{4}(D_b + D_{pi})^2 (v_b + v_i) \times P_{ci} \tag{11}$$

The term, $\frac{\pi}{4}(D_b + D_{pi})^2 (v_b + v_i)$, is the swept volume of a rising bubble (average diameter, D_b; rising velocity, v_b) against settling particles (diameter, D_{pi}; settling velocity, v_i) per unit time.

Particle settling velocity, v_i was calculated based on terminal settling velocity in the stoke region.

The bubble rising velocity, v_b is calculated by equation

$$v_b = \frac{D_{be}}{D_{bh}}\left(\frac{4(\rho_f - LL_{max}) g D_{be}}{3 C_D \rho_f}\right)^{\frac{1}{2}} \tag{12}$$

where LL_{max} is bubble load ($LL_{max} = 0$ is disregard in this calculation), D_{be} is effective bubble diameters, D_{bh} is bubble diameter projected on horizontal plan, ρ_f: Fluid density [kg/m^3], C_D is drag coefficient. $\frac{D_{be}}{D_{bh}}$ is assumed to be 1 for small bubble less than 1 mm in diameter. As C_D is in the function of bubble Reynold number (Re_b), which also depends on bubble rising velocity, calculation approach of C_D was created by the relation between Re_b and C_D is used.

The calculated value of P_{ci} (eq. (5)) and k_i (eq. (11)) as the function of particle diameter (D_{pi}) is shown in Fig. 1 and this value was used in the model calculation. Particle terminal settling velocity (v_i) was calculated from stoke laws based on particle size (D_{pi}) and bubble rising velocity (v_b) was calculated using eq. (12) with bubble diameters, $D_b = 0.9$ mm. Using eq. (8), recovery of target minerals having a particle size distribution η_i, R can be calculated.

4. Results and Discussion

4.1 Flotation of un-agglomerated chalcopyrite

As mentioned in the previous section, the bubble-particle collision probability of fine particles is lower than that of larger particles. As a result, the recovery rate of smaller particles is slower than that of bigger particles. To confirm this particle size effect on flotation recovery, flotation experiments were conducted using ground chalcopyrite samples having different particle sizes ($D_{50} = 3$, 7 and 22 μm). As shown in Fig. 2, Cu recovery increased as particles became larger.

For model calculation, particle size distributions (volume-based) were determined by laser diffraction as illustrated in Fig. 3. Plot (II) in Fig. 3 shows the size distribution curve of particles suspended in water after conditioning with KAX

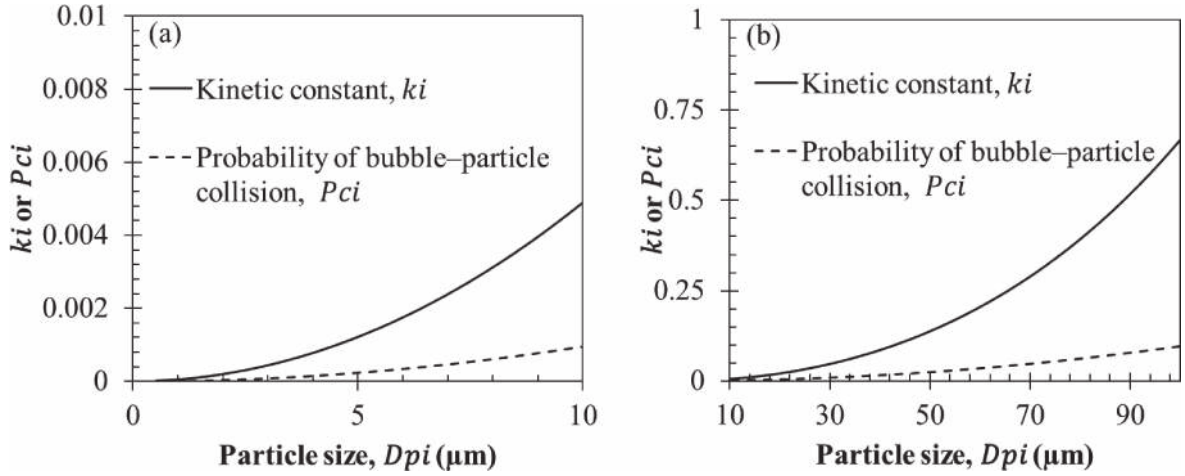

Fig. 1 Probability of bubble-particle collision (P_{ci}) and kinetic constant k_i of particle having diameter D_{pi}: (a) Particle diameter D_{pi} from 0–10 μm and (b) particle diameter D_{pi} from 10–100 μm. Particle terminal settling velocity (v_i) was calculated from stoke laws based on particle size (D_{pi}) and bubble rising velocity (v_b) was calculated using eq. (12) with bubble diameters, $D_b = 0.9$ mm.

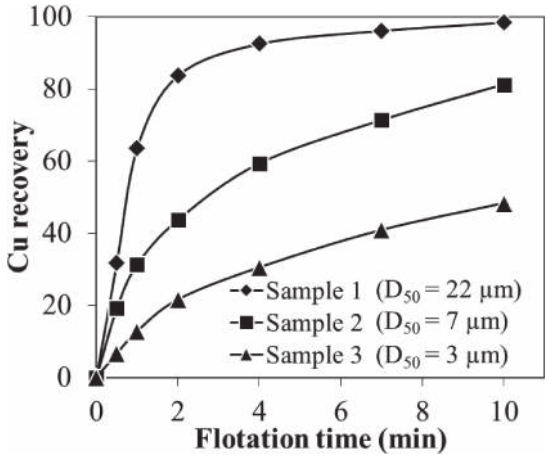

Fig. 2 Copper (Cu) recovery as a function of flotation time using three different size fractions of chalcopyrite: Sample 1 ($D_{50} = 22$ μm), Sample 2 ($D_{50} = 7$ μm), and Sample 3 ($D_{50} = 3$ μm).

just before flotation. For comparison, the size distribution of primary particles (Plot (I) measured in ethanol) were also shown in this figure. By comparing Plots (I) and (II), it was apparent that flocculation occurred by simply conditioning fine chalcopyrite with KAX in the flotation cell. Flocculation occurs due to most likely to hydrophobic attraction of chalcopyrite particles and their increased hydrophobicity via adsorption of KAX. For the kinetic model calculations, the particle size distribution measured after conditioning with KAX (just before flotation) was used.

Figure 4 shows the bubble size distribution (number-based) measured in the flotation cell. As shown in Fig. 3(a), mode (peak) bubble size was around 0.9 mm, and the frequency was more than 30% at this bubble size. From the cumulative size distribution curve (Fig. 4(b)), it was observed that >70% of bubbles were within the size range of 0.8 to 1.0 mm. Based on these results and to simplify the kinetic modeling calculations, the mode bubble size (D_b) of 0.9 mm was used.

The flotation recovery of samples 1, 2 and 3 was calculated as a function of time using the first-order kinetic model described in section 3.2 (solid lines in Figs. 5(a)–(c)). For comparison, experimental results shown in Fig. 2 were also plotted in Fig. 5. The results showed that the first-order kinetic model fitted well with the experimental results, suggesting that this model is applicable for the flotation of un-agglomerated chalcopyrite samples. The similar results were also observed by several authors.[28–30)]

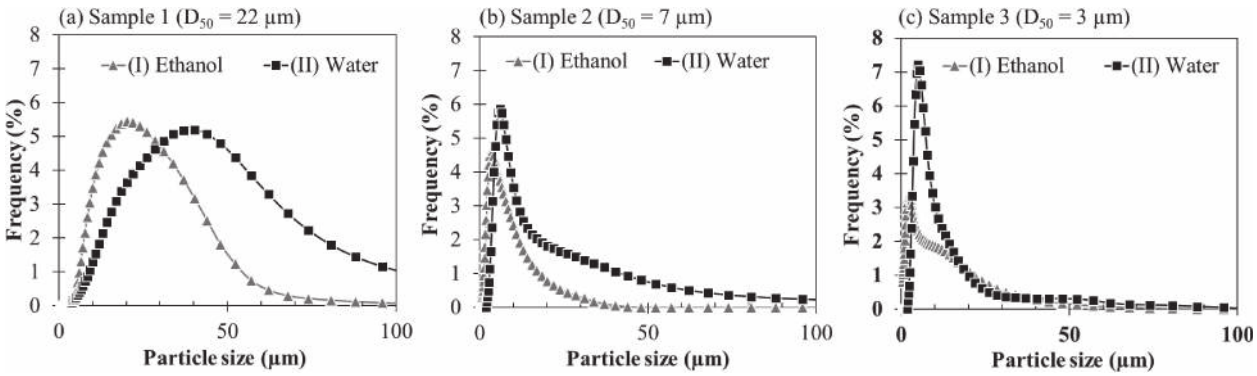

Fig. 3 Particle size distributions of the three samples ((a) Sample 1, (b) Sample 2, and (c) Sample 3) measured in ethanol (I) and water (II) after conditioning.

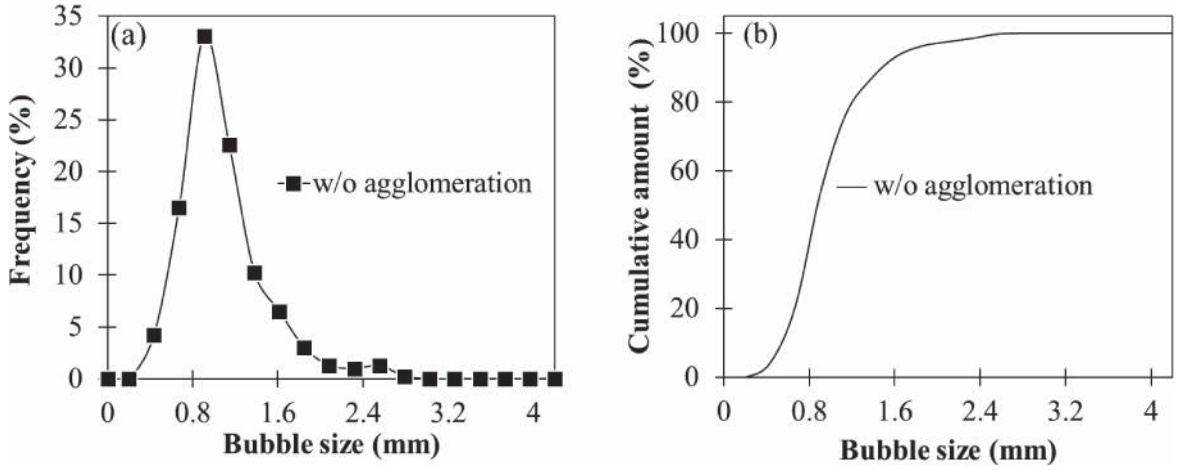

Fig. 4 Bubble size (D_b) distribution measured in the filtered flotation solution without oil agglomeration: (a) Frequency (%) as a function of bubble size, and (b) Cumulative (%) as a function of bubble size.

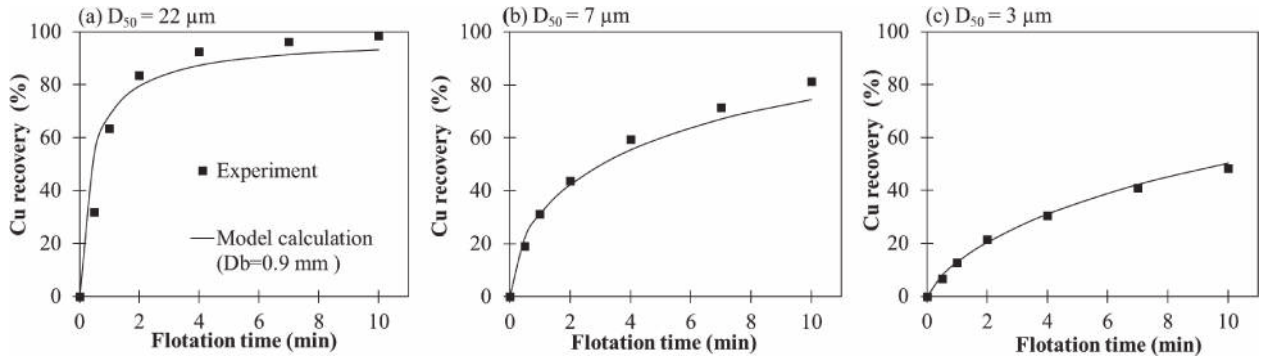

Fig. 5 Comparison between experimental flotation results of samples 1 ($D_{50} = 22\,\mu m$), 2 ($D_{50} = 7\,\mu m$) and 3 ($D_{50} = 3\,\mu m$) and the first-order kinetic model using a bubble size (D_b) of 0.9 mm without agglomeration.

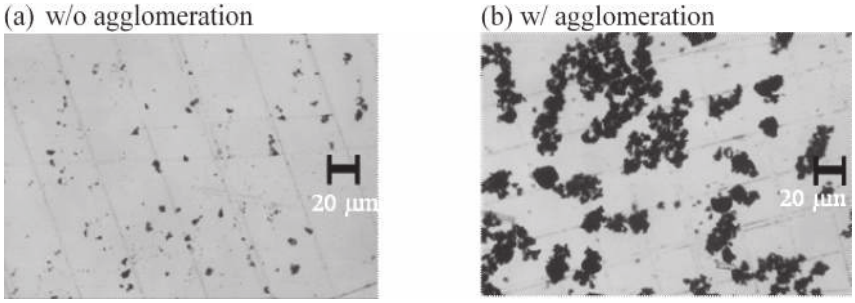

Fig. 6 Photomicrographs of finely ground chalcopyrite w/o agglomeration (a) and w/ agglomeration (b).

4.2 Flotation of agglomerated chalcopyrite

Chalcopyrite sample 3 ($D_{50} = 3\,\mu m$) was used for the agglomeration-flotation tests. Figure 6(a) and 6(b) show photomicrographs of samples before and after agglomeration, respectively and these results confirmed that the size of particles increased after agglomeration. The accurate size distribution of agglomerate could not be determined from this image because of the limitation of resolution of microscopic observation, which may cause the underrating of the amounts of fine particles. So, we used the laser diffraction sizer, which can measure particle size in the range between 0.02 μm to 2800 μm, to determine the agglomerate size distribution. The particle size distributions (volume-based) without and with agglomeration in terms of frequency and cumulative amount are shown in Figs. 7(a) and 7(b), respectively. After agglomeration, the mode particle size increased from 6 to 10 μm and D_{80} increased from 10 μm to 17 μm.

Figure 8 shows the Cu recovery as a function of flotation time with and without agglomeration. Copper recovery increased with agglomeration, which indicates that oil agglomeration is an effective technique to improve Cu recovery of finely ground samples.

To evaluate the applicability of the first-order kinetic model to agglomeration-flotation, this model was fitted with the experimental results. In the first trial of the calculation, we assumed that the bubble size is 0.9 mm, which was the same as that previously used in the kinetic model shown in Fig. 5, and particle size distribution measured after

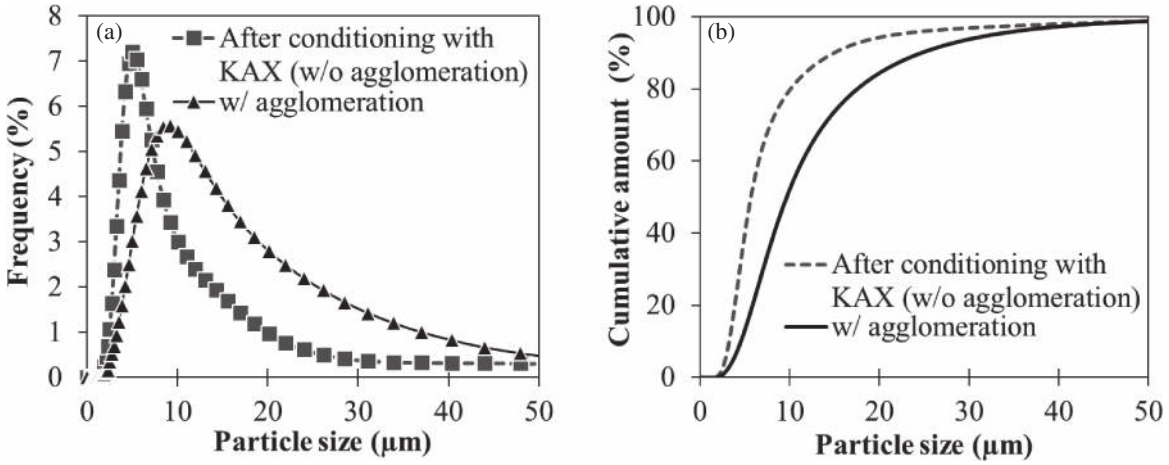

Fig. 7 Particle size distribution of sample 3 ($D_{50} = 3\,\mu m$) after conditioning with KAX (w/o agglomeration) and w/ agglomeration: (a) frequency as a function of particle size, and (b) cumulative amount as a function of particle size.

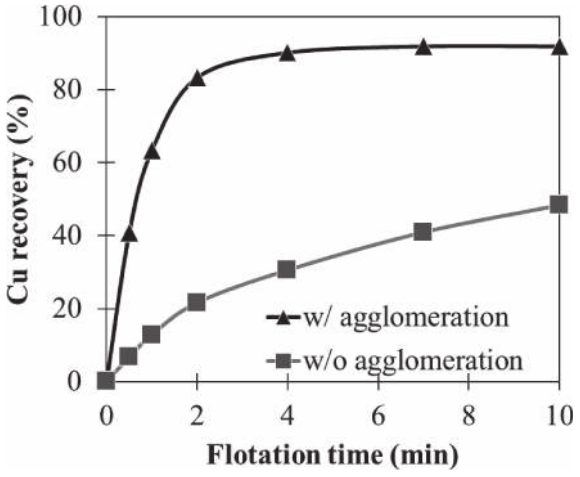

Fig. 8 Copper (Cu) recovery as a function of flotation time of Sample 3 ($D_{50} = 3\,\mu m$) w/o and w/ agglomeration.

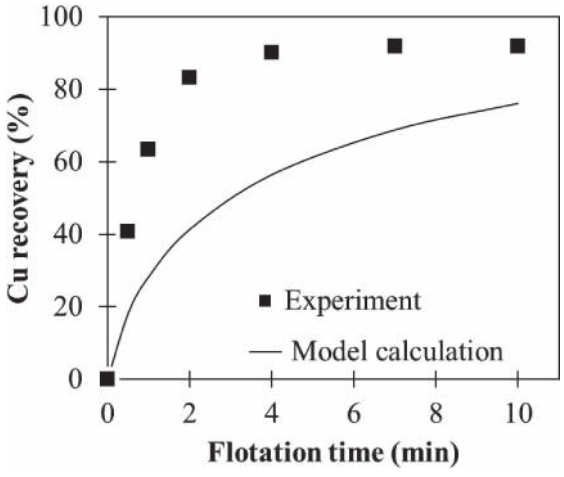

Fig. 9 Comparison between the experimental results of agglomerated chalcopyrite and the first-order kinetic model using a bubble size (D_b) of 0.9 mm.

agglomeration shown in Fig. 6 was used. Although the "apparent" density of agglomerates is lower than a single chalcopyrite grain of the same size because agglomerates contain pores, this was ignored for simplicity and the density of agglomerates was assumed to be equal to that of chalcopyrite (4200 $kg.m^{-3}$).

Figure 9 shows the calculated results (Cu recovery-time curve) for agglomerated chalcopyrite together with the experimental results. The recovery after 10 min calculated from model was 83% but the experimental results was higher at 92%. This discrepancy indicates that the conventional first-order kinetic model for flotation was not applicable for agglomerated chalcopyrite.

It should be noted that experimental Cu recovery was much higher than that predicted by the first-order kinetic model. In the model calculation shown here, the effect of particle size increase was already considered. It has been considered that improved recovery of agglomeration-flotation is due to the increase in particle size. The higher experimental recovery compared with model, therefore, indicates that the increase in particle size alone was not the only reason for the improved flotation after oil agglomeration.

4.3 Factors affecting oil agglomeration-flotation flotation of agglomerated chalcopyrite

As shown in the conventional first-order kinetic model for flotation (eq. (11)), the kinetic constant (k_i) of flotation system depends on particle size (D_{pi}), bubble size (D_b), bubble rising velocity (v_b), settling velocity of agglomerate (v_i) and probability of collision (P_{ci}). In the model calculation shown in Fig. 9, the values used for D_b, v_b and v_i were only assumed, so to improve the model, these values were experimentally determined. In addition, agglomeration in the flotation cell was also investigated.

4.3.1 Bubble size (D_b)

Bubble size is strongly influenced by the surface tension of water-air interface. During agglomeration, the addition of chemical compounds like kerosene may cause the reduction of surface tension, resulting in smaller bubbles. To evaluate the effects of agglomeration on the surface tension, this parameter was measured in the supernatant after agglomeration of chalcopyrite using a Processor Tensiometer (K100MK2, KRUSS, Germany) at 25°C. The agglomeration condition was 200 g/t of KAX, 0.3 mL of kerosene and 30 min of agglomeration time. The filtrate was collected

Table 1 Surface tension of various solutions.

Solutions	Surface tension (mN/m)
DI water	72.3
DI water with MIBC (25μl/l)	71.3
Filtrate of ground chalcopyrite suspension after agglomeration	68.5

using filter paper (5C) and 25 μL/L of MIBC was added before the measurement. As summarized in Table 1, the surface tension of the filtrate of chalcopyrite suspension after agglomeration was slightly lower than those of distilled water with and without MIBC. Lower surface tension for the filtrate after agglomeration may be due to the formation of surface-active reagents from kerosene and KAX during agglomeration with high speed agitation. The lower surface tension may cause the decrease of bubble size in flotation cell.

Bubble size distributions were measured for the filtrate after agglomeration. Figure 10 shows the distribution of bubble size (i.e., diameter) generated in the flotation cell with or without agglomeration after adding 25 μL/L of MIBC as the frother. Although the distribution of bubble size with agglomeration was slightly different compared with the one without agglomeration, the peak bubble size was almost the same (i.e., 0.9 mm) for both cases.

Figure 11 shows the experimental results of flotation for agglomerated chalcopyrite sample with model calculation using different bubble sizes (D_b). To fit the kinetic model with the experimental results, the bubble diameter should be around 0.4 mm. This value is quite different from the actual value shown in Fig. 9 (0.9 mm after agglomeration), indicating that the bubble size was not the main reason for the discrepancy between experimental and kinetic modeling results for agglomerated particles.

4.3.2 Bubble rising velocities (v_b)

Figure 12 shows the relation between diameter and rising velocities of air bubbles generated in the flotation cell with or without agglomeration. The bubble rising velocities were measured in the filtrate of agglomeration suspension after adding 25 μL/L of MIBC. The results showed that the rising velocities of air bubbles in the filtrate of agglomeration suspension were almost the same as that without agglomeration. The rising velocities of bubbles in both cases were consistent with theoretical values calculated by eq. (12). These results imply that the effects of kerosene used in oil agglomeration on the bubble rising velocities were insignif-

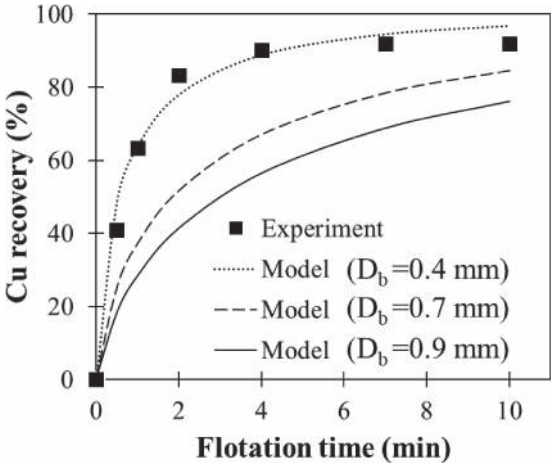

Fig. 11 Comparison between agglomeration-flotation experimental results and the kinetic model using different bubble sizes (D_b) of 0.4, 0.7 and 0.9 mm.

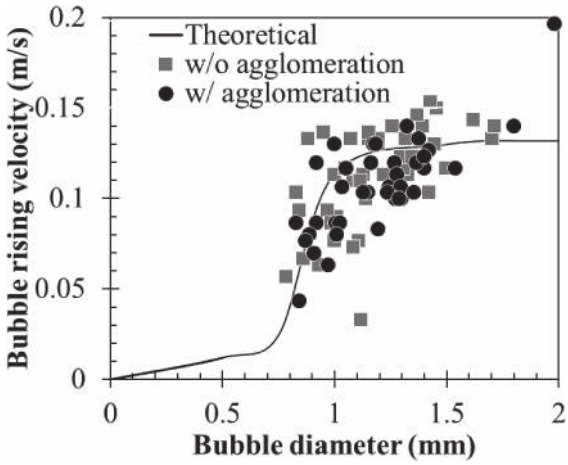

Fig. 12 Experimental and model calculated bubble rising velocities in the flotation suspension w/o and w/ agglomeration.

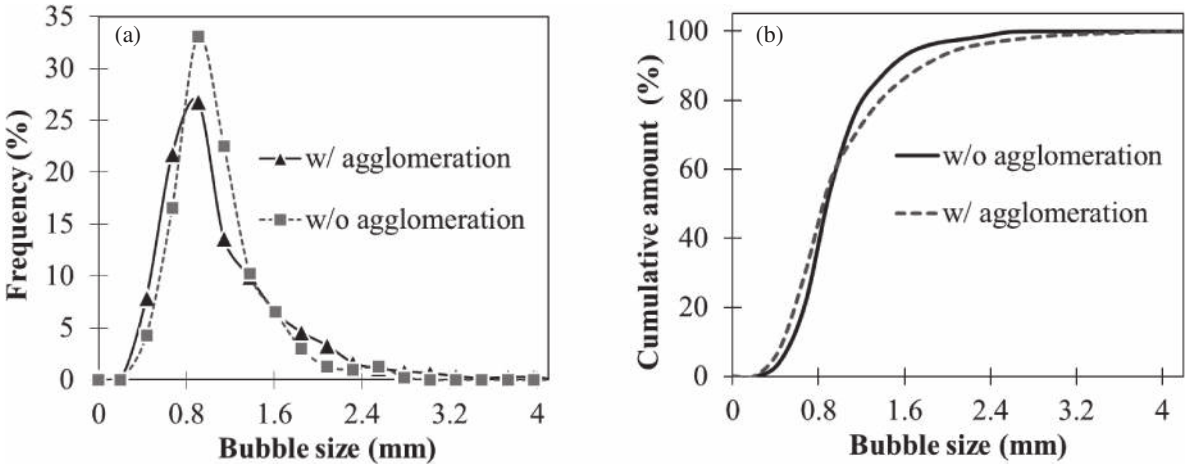

Fig. 10 Bubble size (D_b) distribution of filtrate solution w/ and w/o agglomeration: (a) Frequency (%), (b) Cumulative (%).

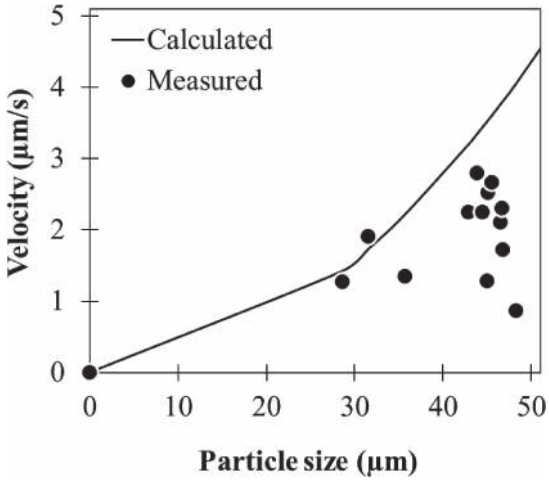

Fig. 13 Measured and calculated settling velocity of agglomerated chalcopyrite.

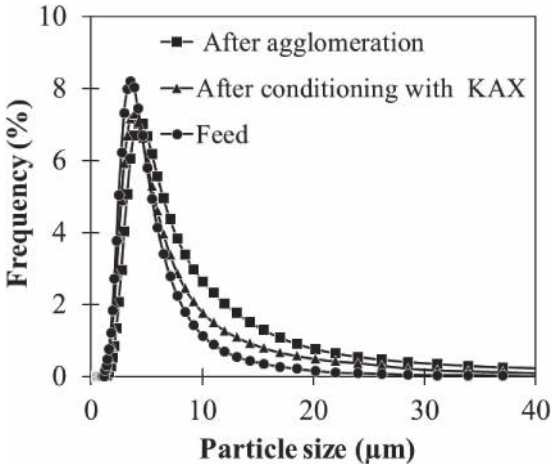

Fig. 14 Changes in the particle size distribution of chalcopyrite in the flotation cell without conditioning, after conditioning with KAX, and after agglomeration for 5 min.

icant. In other words, the changes in bubble rising velocities was not one of the factors that contributed to faster flotation rate of agglomerated particles.

4.3.3 Settling velocities of agglomerates (v_i)

As mentioned previously, the agglomerate's settling velocity was calculated by assuming that its density was equal to that of chalcopyrite. In reality, however, agglomerates of chalcopyrite are porous, so their apparent density is smaller than that of chalcopyrite. Because of the presence of pores, water to pass through agglomerates, which makes the settling behavior of porous and permeable agglomerates different from that of solid, and impermeable particles.[31] These differences may explain the discrepancies observed between the calculated settling velocity and actual velocity. Figure 13 shows the measured value of settling velocity of agglomerated chalcopyrite as a function of diameter of agglomerate. For comparison, calculated values of the settling velocity were also illustrated in this figure. The results showed that agglomerated chalcopyrite settling velocity (SG: 4200 kg·m^{-3}) was lower than the calculated value. As can be seen in eq. (11), the kinetic constant of flotation is influenced by settling velocities (v_i). When the settling velocity, v_i, becomes larger, the bubble swept volume, $\frac{\pi}{4}(D_b + D_{pi})^2(v_b + v_i)$, becomes bigger, which results in faster flotation rates as expressed by eq. (9). As shown in Fig. 13, the measured settling velocity was lower than that of kinetic model calculation, which caused slower flotation rates. In the actual model calculation, however, the slower settling velocity does not have to be considered because the measured settling velocities (v_i) in Fig. 13 (1–5 μm/s) are significantly lower than the bubble rising velocity (v_b) in Fig. 12 (0.02–0.2 m/s). In this case, the bubble swept volume, $\frac{\pi}{4}(D_b + D_{pi})^2(v_b + v_i)$, can be approximated as $\frac{\pi}{4}(D_b + D_{pi})^2 v_b$, which is independent of v_i. Considering the above, it is reasonable to conclude that the differences between measured and calculated settling velocity does not explain the discrepancies of Cu recovery between experimental and kinetic modeling results.

4.4 Agglomeration during flotation

It was assumed in the model calculation that agglomeration does not occur in the flotation cell; that is, the size of an agglomerate remains constant during flotation and is equal to that measured after agglomeration (i.e. before flotation). However, agglomeration during flotation could occur because of mechanical agitation in the flotation cell, which induces either breakage of agglomerates or agglomeration of particles. If this is the case, particle size distribution would change during flotation that may explain the discrepancies between experimental and kinetic modeling results.

To evaluate the possibility of particle size change in the flotation cell, agglomeration in the flotation cell was carried out and the particle size distribution was measured without air bubble introduction. For these measurements, 20 g of chalcopyrite was suspended in 400 mL distilled water in the flotation cell. 200 g/t of KAX was then added and the suspension was stirred for 5 min. After this, 0.3 mL of emulsified kerosene was added, and agglomeration was carried out for 5 min. Figure 14 shows the measured particle size distributions before conditioning with KAX, after conditioning with 200 g/t of KAX, and after agglomeration for 5 min. The amount of coarser size fractions increased after conditioning with KAX, which is likely due to changes in surface wettability of chalcopyrite via KAX adsorption, inducing the natural flocculation of hydrophobic chalcopyrite particles. Further addition of kerosene and 5 min agitation made the particle size even bigger. These results indicate that oil agglomeration occurred in the flotation cell even if the agitation strength was weaker than that of the high-speed mixer used for agglomeration.

To confirm the effects of the agglomeration in flotation cell, flotation experiments were carried out after agglomeration in the flotation cell. As shown in Fig. 15, higher Cu recovery and faster flotation rate were observed after agglomerating in the flotation cell. These results indicate that agglomeration occurred in flotation cell, which caused higher rate and recovery of flotation and explains the discrepancies between experimental and kinetic modeling results noted earlier. This means that agglomeration-flotation could be modeled using a first-order kinetic model by including agglomeration during flotation in the calculations.

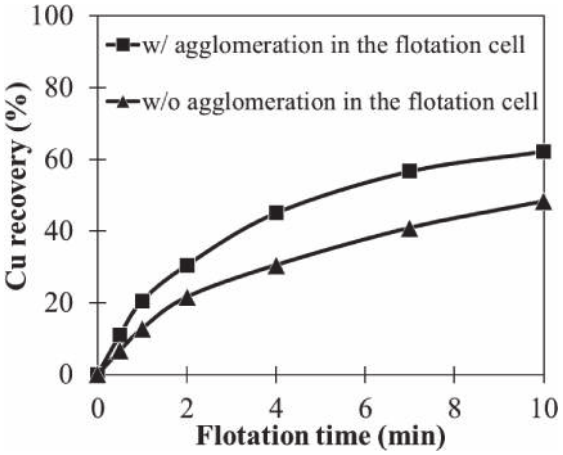

Fig. 15 Changes in the particle size distribution of chalcopyrite in the flotation cell without conditioning, after conditioning with KAX, and after agglomeration for 5 min.

In the future study for the modeling of agglomeration-flotation, the agglomeration in flotation cell should be considered.

5. Conclusions

This study investigated the agglomeration-flotation behavior of finely ground chalcopyrite experimentally using KAX as surface modifier and kerosene as "bridging" liquid and theoretically using first-order kinetic modeling. The results of this study are summarized as follows:

(1) Oil-agglomeration before flotation increased the chalcopyrite particle size (D_{50}) from around 6 to 10 μm that dramatically improved the flotation rate.
(2) Flotation rate that was calculated by first-order kinetic model fitted well with the experimental results of un-agglomerated chalcopyrite.
(3) The conventional first-order kinetic model was insufficient to explain the flotation of agglomerated chalcopyrite and model calculated values did not fit the experimental results.
(4) Bubble size and surface tension, settling rate of agglomerates, bubble rising velocities could not explain the significant deviations between experimental and calculated results.
(5) Agglomeration occurred in the flotation cell even without prior oil agglomeration in a high-speed mixer and was likely the main reason for the discrepancies between experimental and kinetic modeling results of flotation recovery.

Notation

D_{pi}: Diameter of particle type i
D_b: Diameter of bubble
P_A: Probabilities of particle/bubble attachment
P_D: Probabilities of particle/bubble detachment
P_C: Probabilities of particle/bubble collision
G_v: Specific aeration rate
k_i: Kinetic constant of particle type i
n_b: Number of bubbles in flotation cell
η_i: Particle distribution frequency (%) of particle type i
Re_b: Reynold number of bubbles
R: Copper recovery (%)
t: Flotation time (s)
v_b: Bubble rising velocity
v_i: Particle settling velocity

REFERENCES

1) F. Jiangang, C. Kaida, W. Hui, G. Chao and L. Wei: Miner. Eng. **39** (2012) 133–139.
2) W. Trahar: Int. J. Miner. Process. **8** (1981) 289–327.
3) Z. Dai, D. Fornasiero and J. Ralston: Adv. Colloid Interface Sci. **85** (2000) 231–256.
4) T. Miettinen, J. Ralston and D. Fornasiero: Miner. Eng. **23** (2010) 420–437.
5) W.J. Trahar and L.J. Warren: Int. J. Miner. Process. **3** (1976) 103–131.
6) R.H. Yoon: Int. J. Miner. Process. **58** (2000) 129–143.
7) J.A. Finch: Miner. Eng. **8** (1995) 587–602.
8) R.H. Yoon: Miner. Eng. **6** (1993) 619–630.
9) G. Bhaskar Raju and P.R. Khangaonkar: Int. J. Miner. Process. **9** (1982) 133–143.
10) R.T. Rodrigues and J. Rubio: Int. J. Miner. Process. **82** (2007) 1–13.
11) L.J. Warren: J. Colloid Interface Sci. **50** (1975) 307–318.
12) J. Rubio and H. Hoberg: Int. J. Miner. Process. **37** (1993) 109–122.
13) G.C. Sresty and P. Somasundaran: Int. J. Miner. Process. **6** (1980) 303–320.
14) M.I. Alonso, A.F. Valdés, R.M. Martínez-Tarazona and A.B. Garcia: Fuel **78** (1999) 753–759.
15) J.H. Slaghuis and L.C. Ferreira: Fuel **66** (1987) 1427–1430.
16) S. Song, A. Lopez-Valdivieso, J.L. Reyes-Bahena and C. Lara-Valenzuela: Miner. Eng. **14** (2001) 87–98.
17) C.I. House and C.J. Veal: Miner. Eng. **2** (1989) 171–184.
18) C.N. Bensley, A.R. Swanson and S.K. Nicol: Int. J. Miner. Process. **4** (1977) 173–184.
19) E. Sahinoglu and T. Uslu: Fuel **113** (2013) 719–725.
20) K. van Netten, R. Moreno-Atanasio and K.P. Galvin: Chem. Eng. Res. Des. **110** (2016) 54–61.
21) X. Li, N. Hiroyoshi, C.B. Tabelin, K. Naruwa, C. Harada and M. Ito: Chemosphere **214** (2019) 70–78.
22) I. Park, C.B. Tabelin, K. Magaribuchi, K. Seno, M. Ito and N. Hiroyoshi: J. Hazard. Mater. **344** (2018) 322–332.
23) C.B. Tabelin, S. Veerawattananun, M. Ito, N. Hiroyoshi and T. Igarashi: Sci. Total Environ. **580** (2017) 687–698.
24) R.A. Grau and K. Heiskanen: Miner. Eng. **15** (2002) 507–513.
25) R.A. Grau and K. Heiskanen: Miner. Eng. **16** (2003) 1081–1089.
26) R.H. Yoon and G.H. Lutttrell: Miner. Process. Extr. Metall. Rev. **5** (1989) 101–122.
27) R.P. King: *Modeling and Simulation of Mineral Processing Systems*, 1st ed., (Butterworth Heinemann, Oxford, UK, 2001) pp. 312–313.
28) L. Vinnett, M. Alvarez-Silva, A. Jaques, F. Hinojosa and J. Yianatos: Miner. Eng. **77** (2015) 167–171.
29) M. Polat and S. Chander: Int. J. Miner. Process. **58** (2000) 145–166.
30) E. Yalcin and S. Kelebek: Int. J. Miner. Process. **98** (2011) 48–54.